Available online at www.sciencedirect.com
SCIENCE DIRECT®
Applied Surface Science 227 (2004) 349–363
applied surface science
www.elsevier.com/locate/apsusc

Atomistic modeling of solubilization of carbon nanotubes by non-covalent functionalization with poly(*p*-phenylenevinylene-*co*-2,5-dioctoxy-*m*-phenylenevinylene)

M. Grujicic[a,*], G. Cao[a], W.N. Roy[b]

[a]*Program in Materials Science and Engineering, Engineering Innovation Building, Department of Mechanical Engineering, Clemson University, Clemson, SC 29634-0921, USA*

[b]*Army Research Laboratory—Processing and Properties Branch, Aberdeen, Proving Ground, MD 21005-5069, USA*

Received 26 September 2003; received in revised form 10 December 2003; accepted 10 December 2003

Abstract

Molecular dynamics simulations are carried out to analyze the process of solubilization of the armchair, metallic (10,10) single-walled carbon nanotubes (SWCNTs) functionalized with poly(*p*-phenylenevinylene-*co*-2,5-dioctoxy-*m*-phenylenevinylene) (PmPV-DOctOPV) polymer in toluene. Inter- and intra-molecular atomic interactions in the SWCNT + PmPV-DOctOPV + toluene system are represented using condensed-phased optimized molecular potential for atomistic simulation studies (COMPASS), the first ab initio forcefield that enables an accurate and simultaneous prediction of various gas-phase and condensed-phase properties of organic and inorganic materials.

The results obtained shows that due a strong bonding between the SWCNTs and the PmPV-DOctOPV, a homogeneous toluene suspension of the SWCNTs functionalized with PmPV-DOctOPV, obtained via processes such as the sonication, is stable and can be used for separation of the SWCNT bundles into individual nanotubes.

PACS: 81.05.Tp (Fullerenes and related materials)

Keywords: Carbon nanotubes; Molecular dynamics simulations; Functionalization

1. Introduction

Since their discovery in 1991 [1], carbon nanotubes have been investigated very aggressively because of a unique combination of their mechanical, electrical, and chemical properties. Depending on the fabrication method used, carbon nanotubes appear either predominantly as single-walled carbon nanotubes (SWCNTs) or as multi-walled carbon nanotubes (MWCNTs). SWCNTs, predominantly produced in carbon ablation and arc discharge processes, can be described as a single graphene sheets rolled up into a cylinder with a quasi-one-dimensional crystal structure. Depending on their diameter and the spiral conformation (chirality), SWCNTs can be either semiconducting or metallic. Mechanical properties of the SWCNTs are quite remarkable: their elastic modulus is typically above 1 TPa, and they can undergo very large non-uniform

* Corresponding author. Tel.: +1-864-656-5639; fax: +1-864-656-4435.
E-mail address: mica.grujicic@ces.clemson.edu (M. Grujicic).

0169-4332/$ – see front matter © 2004 Elsevier B.V. All rights reserved.
doi:10.1016/j.apsusc.2003.12.018

Report Documentation Page

Form Approved
OMB No. 0704-0188

1. REPORT DATE	2. REPORT TYPE	3. DATES COVERED
2004		**00-00-2004 to 00-00-2004**

4. TITLE AND SUBTITLE
Atomistic modeling of solubilization of carbon nanotubes by non-covalent functionalization with poly(p-phenylenevinylene-co-2,5-dioctoxy-m-phenylenevinylene)

5a. CONTRACT NUMBER

5b. GRANT NUMBER

5c. PROGRAM ELEMENT NUMBER

6. AUTHOR(S)

5d. PROJECT NUMBER

5e. TASK NUMBER

5f. WORK UNIT NUMBER

7. PERFORMING ORGANIZATION NAME(S) AND ADDRESS(ES)
Celmson University,Department of Mechanical Engineering,Clemson,SC,29634

8. PERFORMING ORGANIZATION REPORT NUMBER

9. SPONSORING/MONITORING AGENCY NAME(S) AND ADDRESS(ES)

10. SPONSOR/MONITOR'S ACRONYM(S)

11. SPONSOR/MONITOR'S REPORT NUMBER(S)

12. DISTRIBUTION/AVAILABILITY STATEMENT
Approved for public release; distribution unlimited

13. SUPPLEMENTARY NOTES

14. ABSTRACT
Molecular dynamics simulations are carried out to analyze the process of solubilization of the armchair, metallic (10,10) single-walled carbon nanotubes (SWCNTs) functionalized with poly(p-phenylenevinylene-co-2,5-dioctoxy-m-phenylenevinylene) (PmPV-DOctOPV) polymer in toluene. Inter- and intra-molecular atomic interactions in the SWCNT ? PmPV-DOctOPV ? toluene system are represented using condensed-phased optimized molecular potential for atomistic simulation studies (COMPASS), the first ab initio forcefield that enables an accurate and simultaneous prediction of various gas-phase and condensed-phase properties of organic and inorganic materials. The results obtained shows that due a strong bonding between the SWCNTs and the PmPV-DOctOPV, a homogeneous toluene suspension of the SWCNTs functionalized with PmPV-DOctOPV, obtained via processes such as the sonication, is stable and can be used for separation of the SWCNT bundles into individual nanotubes.

15. SUBJECT TERMS

16. SECURITY CLASSIFICATION OF:			17. LIMITATION OF ABSTRACT	18. NUMBER OF PAGES	19a. NAME OF RESPONSIBLE PERSON
a. REPORT	b. ABSTRACT	c. THIS PAGE			
unclassified	**unclassified**	**unclassified**	**Same as Report (SAR)**	**15**	

(even highly localized) reversible deformations. With an exception of the nanotubes ends, and the location of topological defects (e.g. 7-5-5-7 and Stone-Wales defects), SWCNTs are generally not very reactive. MWCNTs are generally produced during thermal decomposition of gaseous carbon precursors such as methane. Due to a weak inter-wall bonding, MWCNTs have generally inferior mechanical properties relative to those of the SWCNTs. Their electrical properties are similar to those of the SWCNTs, but they could not be easily correlated with their chirality. Chemical properties of MWCNTs are dominated by the structure of their outer wall and are, hence, similar to the ones of the corresponding SWCNTs.

While carbon nanotubes have been perceived as having a great potential in many critical applications (e.g. field-emission flat-panel displays [2]), novel microelectronic devices (e.g. [3]), hydrogen storage devices (e.g. [4]), structural reinforcement agents (e.g. [5]), and chemical and electrochemical sensors (e.g. [6]), the lack of control of their purity and diameter, length, and chirality distributions during fabrication is a major current obstacle to their full utilization. During fabrication of the carbon nanotubes, other materials such as carbon onions and turbostratic/amorphous graphite are also generally produced. Many techniques (e.g. oxidation) have been proposed for separation of the carbon nanotubes from the unwanted byproducts. However, a method is currently lacking for separation of the carbon nanotubes according to their diameter and/or chirality, the key geometrical and structural parameters which control electronic properties of these materials.

Recently, a new approach for carbon nanotube separation and purification has been demonstrated [7]. The method is based on non-covalent sidewall functionalization (attachment of the functional groups/molecules on the outer wall) of SWCNTs and MWCNTs with π-conjugated poly(*p*-phenylenevinylene-*co*-2,5-dioctoxy-*m*-phenylenevinylene) (PmPV-*co*-DOctOPV) polymer. Pristine carbon nanotubes, despite their hydrophobic character, are found not to be soluble in non-polar solvents such as toluene. However, after functionalization with the PmPV-*co*-DOctOPV, carbon nanotubes become soluble and can be "permanently" suspended in toluene. While the solubilization of carbon nanotubes through sidewall functionalization can be achieved in many different ways, it is critical that functionalization is of a non-covalent character so that the electronic characteristics of the carbon nanotubes (governed by their sp^2 hybridization) are not altered.

π-Conjugated polymers, also known as semiconducting polymers, are characterized by alternating single and double bonds between carbon atoms along the polymer backbone. The π-conjugated polymer with the simplest chemical structure is *polyacetylene* (the backbone structure: –C=C–C=C–C=C). Since the energy of the π-electrons in double bonds is much higher than the energy of the electrons in single bonds, electrons can easily move from one double bond to the adjacent single bond making the π-conjugated polymers one-dimensional organic semiconductors. Consequently, π-conjugated polymers have many interesting properties such as: (a) they can emit light, the color of which is tailorable through modifications in the chemical structure; (b) they can generate electric current upon absorbing light, and hence can be used in photovoltaic devices; and (c) as in other semiconductors, the conductivity in π-conjugated polymers can be modified by varying the level of doping. In general, the doping level depends on the oxidation state of the polymer, which can be electrochemically controlled. When the oxidation level is varied by the application of electrical potential, many of the materials properties change, such as; volume (leads to the use of π-conjugated polymers in actuator applications), color (leads to the application of these materials in electrochromic windows and displays), mechanical properties, and hydrophobicity. The presence of double bonds makes π-conjugated polymers very reactive and, hence, suitable for functionalization of the carbon nanotubes through p_z–p_z electron interactions between the polymers and the outer walls of the nanotubes.

In a series of papers, Blau and co-workers [7–16] carried out a detailed experimental and computational investigation of solubilization of the SWCNTs and MWCNTs (sidewall) functionalized with PmPV-DOctOPV in toluene. Their atomistic simulation results showed that the backbone of the PmPV-DOctOPV molecule adopts a relatively flat helical structure which is governed by the *m*-phenylene linkage. van der Waals interactions between the octyloxy groups, on the other hand, cause these groups to project outwards from the helical structure. This PmPV-DOctOPV conformation is shown to promote

adhesion of these molecules to the nanotubes and, hence, is believed to play a critical role in the nanotubes solubilization process. While the work of Blau and co-workers [7–16] has resulted in a major improvement of our understanding of nanotubes solubilization with sidewall functionalization, two important points were not addressed in their work: (a) why hydrophobic nanotubes are not soluble in non-polar solvents like toluene; and (b) what is the role of the solvent in nanotubes solubilization by sidewall functionalization. The problem of a lack of solubilization of carbon nanotubes in toluene has been address in our recent paper [17]. It was found that the introduction of carbon nanotubes into toluene gives rise to a major reorganization of the toluene molecules surrounding the nanotubes. The associated decrease in the configurational entropy of toluene causes the solvation Gibbs free energy to become positive rendering the suspension of carbon nanotubes in toluene, obtained by processes such as the sonication of carbon nanotube bundles in toluene, unstable. In the present work, we use atomistic simulations to investigate the interactions between different PmPV-DOctOPV conformations and SWCNTs in vacuum and in toluene in order to examine the role of toluene in functionalization-assisted nanotubes solubilization. While chirality of the SWCNTs can generally play a role, the results obtained in the present work show that the chirality effect is relatively small. Hence, only the results pertaining to armchair metallic (10,10) SWCNTs are presented in this paper.

The organization of the paper is as follows: a brief overview of the PmPV-DOctOPV conformations, the computational cell, the computational method, and the inter-atomic forcefield potentials used in the present work are presented in Section 2. The main results obtained in the present work are presented and discussed in Section 3, while the key conclusions resulted from the present study are summarized in Section 4.

2. Computational procedure

2.1. PmPV-DOctOPV conformations

As shown in Fig. 1, PmPV-DOctOPV is a π-conjugated polymer and is a substituted form of the poly(*p*-phenylenevinylene) (PPV) with an added dihedral angle that helps the PmPV-DOctOPV polymer chains spiral into a helical structure. In sharp contrast, the PPV chains are essentially linear with a slight twist along the chain backbone. Molecular mechanics calculations [18] showed that the PmPV-DOctOPV helix structure appears in two distinct low energy configurations in vacuum: (a) an ~1.8 nm diameter helical configuration with an ~0.6 nm pitch which involves five PmPV-DOctOPV monomers per helix turn and (b) an ~0.9 nm diameter configuration with an ~0.9 nm pitch based on four PmPV-DOctOPV monomer units per helix turn. The monomer energy in the larger diameter (generally referred to as the ''loose'' PmPV-DOctOPV) configuration is found to be lower by ~0.88 kJ/mol than the corresponding quantity in the smaller diameter (generally referred to as the ''tight'' PmPV-DOctOPV). While this energy difference is relatively small, interactions between the adjacent octyloxy side-groups, which are more pronounced in the loose PmPV-DOctOPV, further reduces the energy of this configuration relative to that in the tight PmPV-DOctOPV by ~7.5 kJ/mol. In both cases, the helical conformation of the PmPV-DOctOPV is such that a fairly unhindered access to the aromatic rings of the chain backbone is allowed. Optimized molecular structures of the loose and the tight PmPV-DOctOPV conformations [18] showed that the interior of the helixes is not hollow, but rather contains octyloxy side groups. This finding suggests that the mechanism for carbon nanotubes solubilization by simple wrapping of the PmPV-DOctOPV molecules around the nanotubes during sonication of carbon nanotube containing powder in a PmPV-DOctOPV-toluene solution [19] may not be based on the energetically most favorable conformation of the PmPV-DOctOPV. Nevertheless, sonication-assisted formation of the strained PmPV-DOctOPV helixes cannot be excluded. As mentioned earlier, computational investigations carried out by Blau and co-workers [7–16] showed that the backbone of PmPV-DOctOPV molecules in the vicinity of SWCNTs in vacuum adopts a relatively flat helical structure.

Based on the discussion presented in this section, the following three PmPV-DOctOPV conformations have been chosen for use in present atomistic modeling work; (a) loose, (b) tight, and (c) flat.

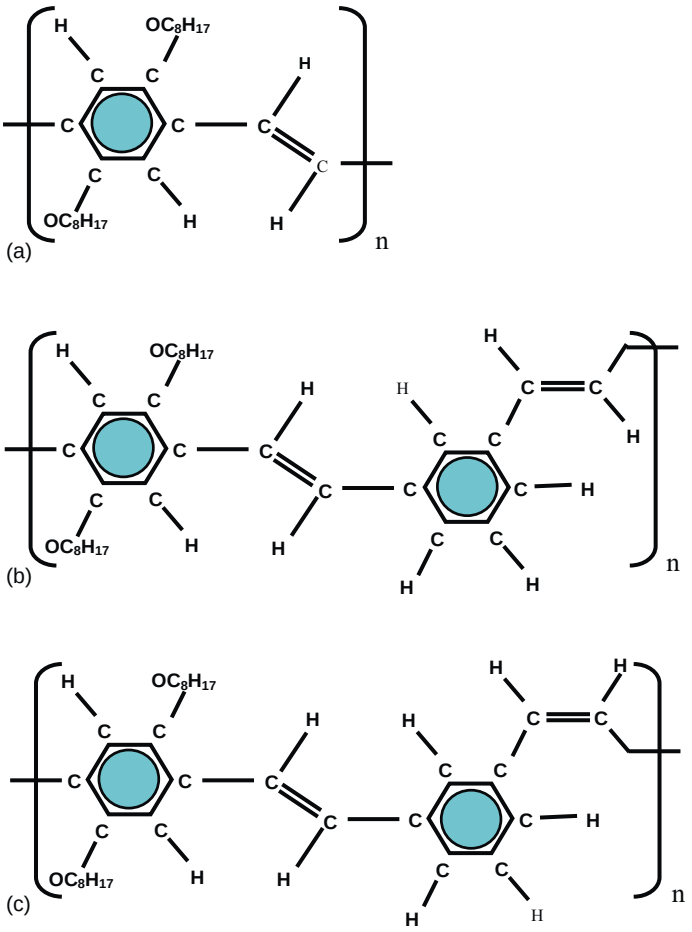

Fig. 1. Chemical structures of: (a) poly(*p*-phenylenevinylene) (PPV) and (b) transoidal (*trans*), and (c) cisoidal (*cis*) forms of the poly-(*p*-phenlyenevinylene-*co*-2,5-dioctoxy-*m*-phenylenevinylene) (PmPV-DOctOPV) monomers.

2.2. Computational cell

Computation of the loose, tight, and flat helical PmPV-DOctOPV conformations in the presence of a single (10,10) SWCNT in vacuum is carried out using rectangular computation cells whose dimensions in the three principal directions are given in Table 1. Also given in Table 1 are the numbers of atoms in the computational cells in each case.

Computations involving the loose, tight, and flat PmPV-DOctOPV conformations in the presence of a SWCNT suspended in toluene are also carried out using rectangular computational cells whose dimensions and the numbers of atoms involved are also listed in Table 1.

Also given in Table 1 are the dimensions and the numbers of atoms in the unit cells used to compute the energies of the three PmPV-DOctOPV conformations in vacuum and in toluene (in the absence of SWCNTs), as well as the dimensions and the numbers of atoms in the unit cell used to compute the energy of a SWCNT in vacuum and in toluene. These values were needed during the calculation of the PmPV-DOctOPV/SWCNT/toluene binding energies.

Periodic boundary conditions are applied in all cases in all three principal directions, with the axis of a (10,10) SWCNT aligned in the z-direction and placed in the center of the computational cell. Thus, the SWCNT is considered as infinitely long and the end-effects associated with its hemispherical caps are

Table 1
Lattice parameters and numbers of atoms involved in different atomistic simulations carried out in the present work

Model	Computational cell			Number of atoms
	a (nm)	*b* (nm)	*c* (nm)	
SWCNT	6.0	6.0	1.955	320
SWCNT + toluene	6.315	6.315	1.955	6,710
Loose PmPV-DOctOPV	6.000	6.000	1.955	1170
Tight PmPV-DOctOPV	6.000	6.000	1.955	624
Flat PmPV-DOctOPV	6.000	6.000	1.955	156
Loose PmPV-DOctOPV + SWCNT	6.000	6.000	1.955	1,490
Tight PmPV-DOctOPV + SWCNT	6.000	6.000	1.955	944
Flat PmPV-DOctOPV + SWCNT	6.000	6.000	1.955	476
Loose PmPV-DOctOPV + toluene	7.049	6.246	1.955	7,560
Tight PmPV-DOctOPV + toluene	6.876	6.246	1.955	7,014
Flat PMPV-DOctOPV + toluene	6.286	6.286	1.955	6,546
Loose PmPV-DOctOPV + SWCNT + toluene	9.160	9.160	1.955	14,270
Tight PmPV-DOctOPV + SWCNT + toluene	9.101	9.101	1.955	13,724
Flat PmPV-DOctOPV + SWCNT + toluene	8.829	8.829	1.955	13,256

neglected. The end effects are generally considered to play a minor role in the SWCNT solubilization process due to a very large (ca. 100–1000) length-to-diameter aspect ratio in SWCNTs. The lengths of the computational cell in the *x*- and *y*-directions are sufficiently large that the interactions between the SWCNTs in the adjacent cells can be neglected.

2.3. Computational method

Interactions of different conformations of PmPV-DOctOPV with a single (10,10) SWCNT in vacuum and in toluene solvent, discussed in the previous section, are modeled using classical molecular dynamics simulations in the microcanonical (NVE) ensemble. To ensure stability of the simulations and energy conservation, a constant time step of 0.2 fs is used for numerical integration of the equations of motion.

After placing the nanotube, PmPV-DOctOPV and toluene molecules into the computational cell, the canonical (NVT) molecular simulations are first carried out for 5 ps until the system is equilibrated at a desired temperature of 295 K. Temperature control is achieved by velocity scaling which was carried out every 1 fs. Once the system is equilibrated, microcanonical (NVE) simulations are carried out for additional 5 ps and the data colleted for computation of the average system properties.

2.4. Forcefield

While accurate simulations of a system of interacting particles generally entail the application of quantum mechanical techniques, such techniques are computationally quite expensive and are usually feasible only in systems containing up to few hundreds of interacting particles. In addition, the main goal of simulations of the systems containing a large number of particles is generally to obtain the systems' bulk properties which are primarily controlled by the location of atomic nuclei and the knowledge of the electronic structure, provided by the quantum mechanic techniques, is not critical. Under these circumstances, a good insight into the behavior of a system can be obtained if a reasonable, physically-based approximation of the potential (forcefield) in which atomic nuclei move is available. Such a forcefield can be used to generate a set of system configurations which are statistically consistent with a fully quantum mechanical description.

As stated above, a crucial point in the atomistic simulations of multi-particle systems is the choice of the forcefields which describe, in an approximate manner, the potential energy hyper-surface on which the atomic nuclei move. In other words, the knowledge of forcefields enables determination of the potential energy of a system in a given configuration. Since currently, a relatively large number of different

forcefield formalisms is being used, a brief overview of the approach used in the present work is given in this section.

In general, the potential energy of a system of interacting particles can be expressed as a sum of the valence (or bond), E_{valence}, cross-term, $E_{\text{cross-term}}$, and non-bond, $E_{\text{non-bond}}$, interaction energies as:

$$E_{\text{total}} = E_{\text{valence}} + E_{\text{cross-term}} + E_{\text{non-bond}} \quad (1)$$

The valence energy generally includes a bond stretching term, E_{bond}, a two-bond angle term, E_{angle}, a dihedral bond-torsion term, E_{torsion}, an inversion (or an out-of-plane interaction) term, E_{oop}, and a Urey–Bradlay term (involves interactions between two atoms bonded to a common atom), E_{UB}, as:

$$E_{\text{valence}} = E_{\text{bond}} + E_{\text{angle}} + E_{\text{torsion}} + E_{\text{oop}} + E_{\text{UB}} \quad (2)$$

A schematic explaining the first four types of valence atomic interactions is given in Fig. 2. The cross-term interacting energy, $E_{\text{cross-term}}$, accounts for the effects such as bond lengths and angles changes caused by the surrounding atoms and generally includes: stretch–stretch interactions between two adjacent bonds, $E_{\text{bond–bond}}$, stretch–bend interactions between a two-bond angle and one of its bonds, $E_{\text{bond–angle}}$, bend–bend interactions between two valence angles associated with a common vertex atom, $E_{\text{angle–angle}}$, stretch–torsion interactions between a dihedral angle and one of its end bonds, $E_{\text{end\_bond–torsion}}$, stretch–torsion interactions between a dihedral angle and its middle bond, $E_{\text{middle\_bond–torsion}}$, bend-torsion interactions between a dihedral angle and one of its valence angles, $E_{\text{angle–torsion}}$, and bend–bend–torsion interactions between a dihedral angle and its two valence angles, $E_{\text{angle–angle–torsion}}$, terms as:

$$\begin{aligned} E_{\text{cross-term}} = {} & E_{\text{bond–bond}} + E_{\text{angle–angle}} + E_{\text{bond–angle}} \\ & + E_{\text{end\_bond–torsion}} + E_{\text{middle\_bond–torsion}} \\ & + E_{\text{angle–torsion}} + E_{\text{angle–angle–torsion}} \end{aligned} \quad (3)$$

The non-bond interaction term, $E_{\text{non-bond}}$, accounts for the interactions between non-bonded atoms and includes the van der Waals energy, E_{vdW}, the Coulomb electrostatic energy, E_{Coulomb}, and the hydrogen bond energy, $E_{\text{H-bond}}$, as:

$$E_{\text{non-bond}} = E_{\text{vdW}} + E_{\text{Columb}} + E_{\text{H-bond}} \quad (4)$$

Inter- and intra-molecular atomic interactions in the PmPV-DOctOPV + SWCNT + toluene system described in the previous section are modeled using condensed-phased optimized molecular potential for atomistic simulation studies (COMPASS), the first ab initio forcefield that enables an accurate and simultaneous prediction of various gas-phase and condensed-phase properties of organic and inorganic materials [20–22]. The COMPASS forcefield uses the following expression for various components of the potential energy:

$$\begin{aligned} E_{\text{bond}} = {} & \sum_{b} [K_2(b - b_0)^2 + K_3(b - b_0)^3 \\ & + K_4(b - b_0)^4] \end{aligned} \quad (5)$$

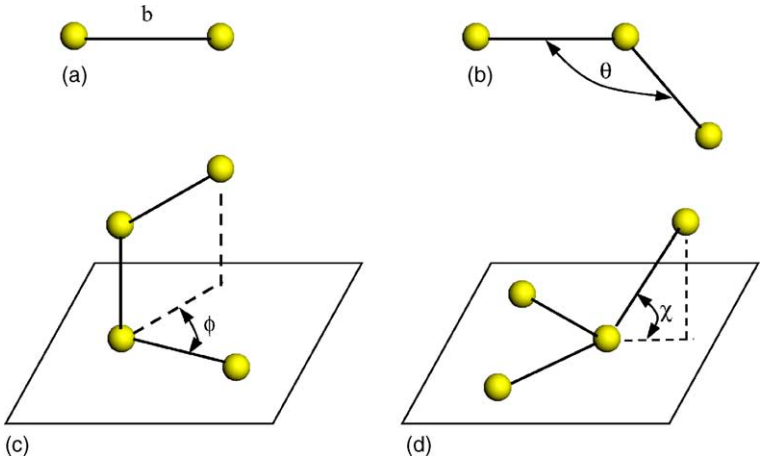

Fig. 2. A schematic of the: (a) stretch; (b) angle; (c) torsion; and (d) inversion valence atomic interactions.

$$E_{\text{angle}} = \sum_{\theta}[H_2(\theta-\theta_0)^2 + H_3(\theta-\theta_0)^3 + H_4(\theta-\theta_0)^4] \quad (6)$$

$$E_{\text{torsion}} = \sum_{\phi}[V_1[1-\cos(\phi-\phi_1^0)] + V_2[1-\cos(2\phi-\phi_2^0)] + V_3[1-\cos(3\phi-\phi_3^0)]] \quad (7)$$

$$E_{\text{oop}} = \sum_{x} K_x \chi^2 \quad (8)$$

$$E_{\text{bond-bond}} = \sum_{b}\sum_{b'} F_{bb'}(b-b_0)(b'-b_0') \quad (9)$$

$$E_{\text{angle-angle}} = \sum_{\theta}\sum_{\theta'} F_{\theta\theta'}(\theta-\theta_0)(\theta'-\theta_0') \quad (10)$$

$$E_{\text{bond-angle}} = \sum_{b}\sum_{\theta} F_{b\theta}(b-b_0)(\theta-\theta_0) \quad (11)$$

$$E_{\text{end\_bond-torsion}} = \sum_{b}\sum_{\phi} F_{b\phi}(b-b_0) \times [V_1\cos\phi + V_2\cos 2\phi + V_3\cos 3\phi] \quad (12)$$

$$E_{\text{middle\_bond-torsion}} = \sum_{b'}\sum_{\phi} F_{b'\phi}(b'-b_0')(b'-b_0') \times [F_1\cos\phi + F_2\cos 2\phi + F_3\cos 3\phi] \quad (13)$$

$$E_{\text{angle-torsion}} = \sum_{\theta}\sum_{\phi} F_{\theta\phi}(\theta-\theta_0)[V_1\cos\phi + V_2\cos 2\phi + V_3\cos 3\phi] \quad (14)$$

$$E_{\text{angle-angle-torsion}} = \sum_{\phi}\sum_{\theta}\sum_{\theta'} K_{\phi\theta\theta'}\cos\phi(\theta-\theta_0) \times (\theta'-\theta_0') \quad (15)$$

$$E_{\text{Coulomb}} = \sum_{i>j}\frac{q_i q_j}{\varepsilon r_{ij}} \quad (16)$$

$$E_{\text{vdW}} = \sum_{i>j}\left[\frac{A_{ij}}{r_{ij}^9} - \frac{B_{ij}}{r_{ij}^6}\right] \quad (17)$$

where b and b' are the bond lengths, θ the two-bond angle, ϕ the dihedral torsion angle, χ the out of plane angle, q the atomic charge, ε the dielectric constant, r_{ij} the i–j atomic separation distance. b_0, K_i ($i=2-4$), θ_0, H_i ($i=2-4$), ϕ_i^0 ($i=1-3$), V_i ($i=1-3$) $F_{bb'}$, b_0', $F_{\theta\theta'}$, θ_0', $F_{b\theta}$, $F_{b\phi}$, $F_{b'\phi}$, F_i ($i=1-3$), $F_{\theta\phi}$, $K_{\phi\theta\theta'}$, A_{ij}, and B_{ij} are the system dependent parameters implemented into discover [20], the atomic simulation program used in the present work.

3. Results and discussion

3.1. PmPV-DOctOPV conformations

3.1.1. PmPV-DOctOPV conformations in vacuum

Atomistic simulations carried in the present work yielded the loose, tight, and flat PmPV-DOctOPV conformations in vacuum. However, the corresponding atomic configurations are not shown here for two reasons; (a) these results are very similar to their counterparts reported in refs. [8,18], (b) these results are also very similar to the PmPV-DOctOPV conformations in the vicinity of a SWCNT in vacuum discussed in the next section.

3.1.2. PmPV-DOctOPV + SWCNT conformations in vacuum

Snapshots of the loose, tight, and flat PmPV-DOctOPV conformations in the vicinity of a SWCNT in vacuum are shown in Figs. 3–5, respectively. In each case, the molecular configuration shown in part (a) of a figure is associated with a view along the nanotube axis while the molecular configuration displayed in part (b) of the same figure corresponds to a view normal to the nanotube axis. To improve clarity of the ball-and-stick (atom-and-bond) molecular configurations shown in Figs. 3–5, carbon atoms in the PmPV-DOctOPV are shown as gray spheres, oxygen atoms as bright larger spheres while hydrogen atoms are not displayed and instead only the bonds involving hydrogen atoms are shown. Carbon atoms in the SWCNT are not shown and instead only carbon–carbon bonds are displayed as solid lines.

While the details of the molecular configurations shown in Figs. 3–5 differ for different PmPV-DOctOPV conformations, few common features can be established: (a) in all cases, the PmPV-DOctOPV conformation exposes the polymer backbone to the SWCNT wall; (b) some of the octyloxy groups tend to wrap around the nanotube; and (c) the remaining octyloxy groups tend to project outward from the SWCNT.

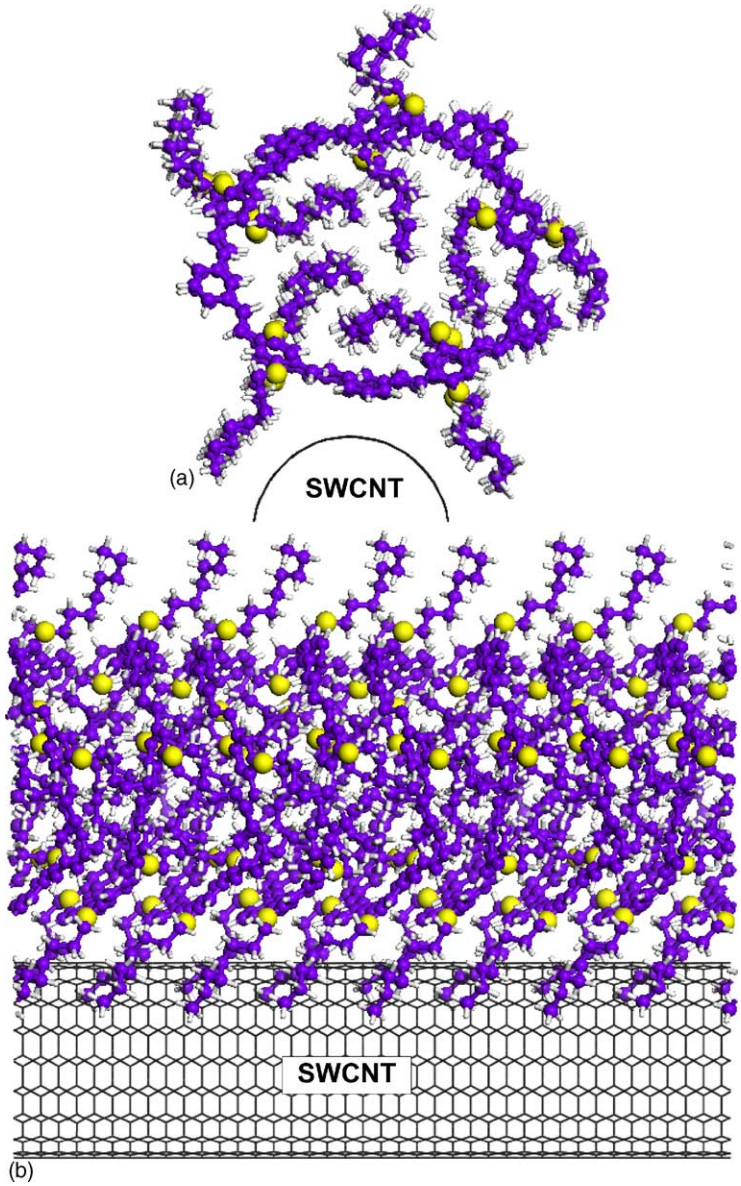

Fig. 3. Loose PmPV-DOctOPV conformation near a (10,10) SWCNT: (a) a view along the SWCNT axis and (b) a view normal to the SWCNT axis.

3.1.3. PmPV-DOctOPV conformations in toluene

Toluene ($C_6H_5CH_3$) is the simplest alkyl benzene, the methylbenzene, in which one of the hydrogen atoms in the benzene (C_6H_6) is replaced by a methyl group (CH_3). At room temperature, toluene is in liquid state. The geometrically optimized structure of toluene along with the atomic charges is shown in Fig. 6. Atomistic simulations carried in the present work yielded the loose, tight, and flat PmPV-DOctOPV conformations in toluene. However, the corresponding atomic configurations are not shown here because they are very similar to the corresponding PmPV-DOctOPV conformations in vacuum.

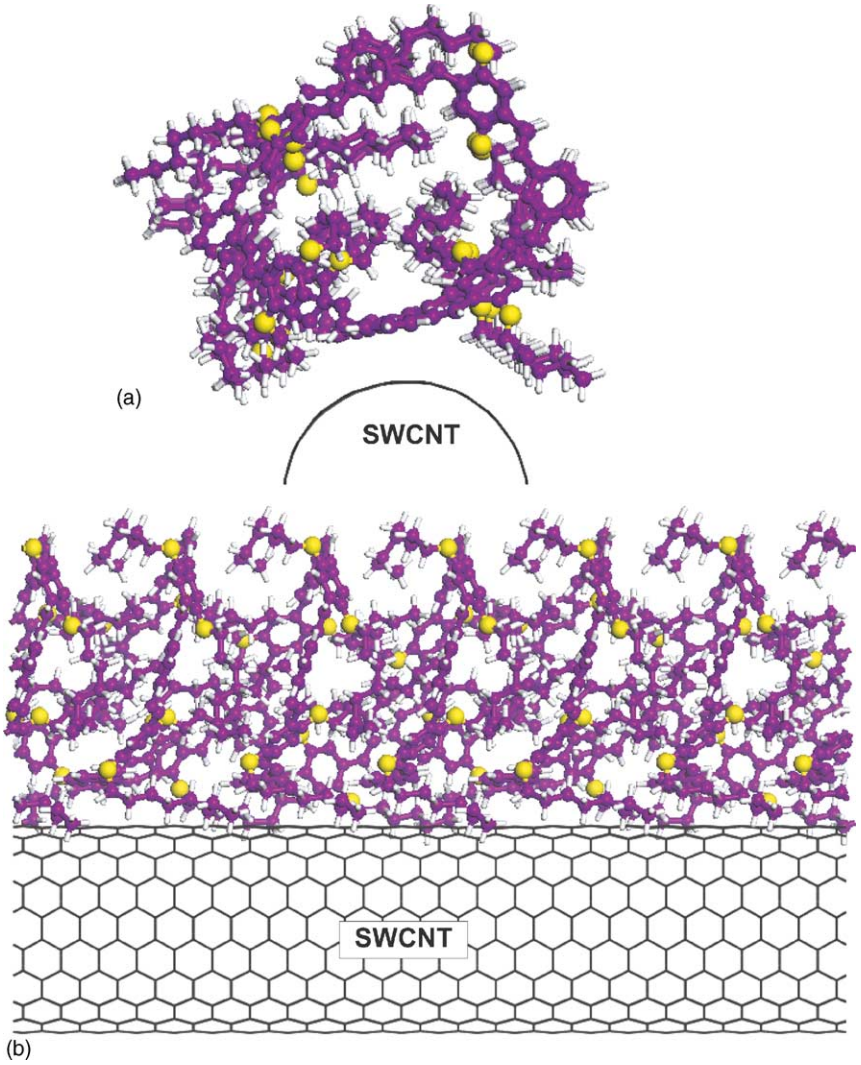

Fig. 4. Tight PmPV-DOctOPV conformation near a (10,10) SWCNT: (a) a view along the SWCNT axis and (b) a view normal to the SWCNT axis.

3.1.4. PmPV-DOctOPV + SWCNT conformations in toluene

Snapshots of the loose, tight, and flat PmPV-DOctOPV conformations in the vicinity of a SWCNT in toluene are shown in Figs. 7–9, respectively. To enhance clarity of the atomistic configurations shown in these figures, the following is done: (a) toluene molecules are displayed using a small-size ball-and-stick representation; (b) a large-size ball-and-stick representation is used to display the PmPV-DOctOPV molecules and the SWCNTs; (c) only a central portion of the unit cell is displayed in each case; and (d) only views along the nanotube axis are shown in Figs. 7–9.

A visual examinations of the atomistic configurations shown in Figs. 7–9 and their comparison with the atomistic configurations displayed in Figs. 3–5 suggests that the presence of toluene does not have a major effect of the conformation of PmPV-DOctOPV near the SWCNTs. However, a comparison of the toluene structure surrounding the SWCNT in Figs. 7–9 with the one observed in the absence of PmPV-DOctOPV (the results given in our recent

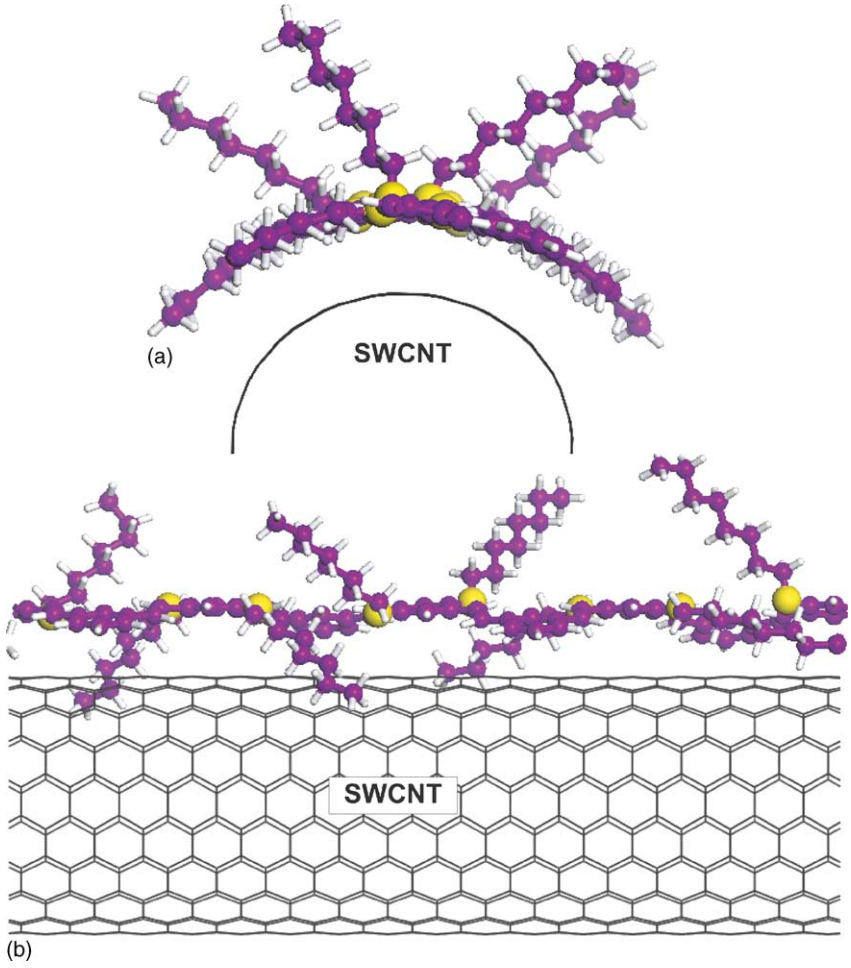

Fig. 5. Flat PmPV-DOctOPV conformation near a (10,10) SWCNT: (a) a view along the SWCNT axis and (b) a view normal to the SWCNT axis.

work [17]), shows that PmPV-DOctOPV disrupts the reorganization of the toluene molecules around the SWCNTs. This finding suggests that the presence of PmPV-DOctOPV gives rise to an increase in the configurational entropy of the toluene in the region surrounding the SWCNTs.

3.2. PmPV-DOctOPV-assisted solubilization of the SWCNTs

3.2.1. Interactions between the PmPV-DOctOPV and the SWCNTs in vacuum

In order to reveal the role of toluene in solubilization process of the SWCNTs functionalized with PmPV-DOctOPV, the binding energy between a PmPV-DOctOPV molecule and a SWCNT is first computed using the following relation:

$$E_{\text{bind}} = E_{\text{PmPV+SWCNT}} - E_{\text{SWCNT}} - E_{\text{PmPV}} \tag{18}$$

where the subscripts bind, PmPV+SWCNT, SWCNT, and PmPV are used to denote the binding, PmPV-DOctOPV + SWCNT complex, SWCNT, and PmPV-DOctOPV energies, respectively. Eq. (18) is used to compute E_{bind} for all three conformations of the PmPV-DOctOPV and the results expressed with respect to a single monomer of the PmPV-DOctOPV. The results of this calculation are displayed in Table 2. It is seen that the binding energy is negative for all

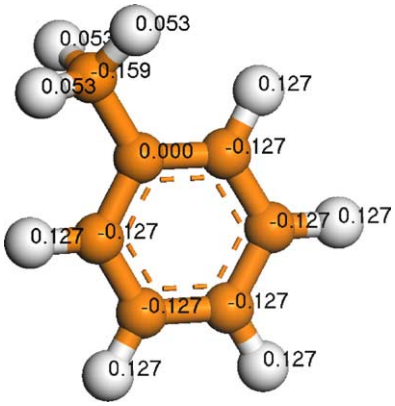

Fig. 6. Geometrically optimized structure of a toluene molecule and the corresponding atomic charges.

three conformations of the PmPV-DOctOPV. Thus, based on the energy consideration only, each of the three PmPV-DOctOPV conformations is attracted to the SWCNTs in vacuum. In addition, in full agreement with the calculations of in het Panhuis et al. [8], the flat conformation is the most stable in the presence of the SWCNTs. Contrary, this conformation is the least stable when present in the form of isolated molecules in vacuum.

3.2.2. Interactions between the PmPV-DOctOPV and the SWCNTs in toluene

The results presented in the previous section suggest that PmPV-DOctOPV in any of the three conformations is attracted to the SWCNTs in vacuum.

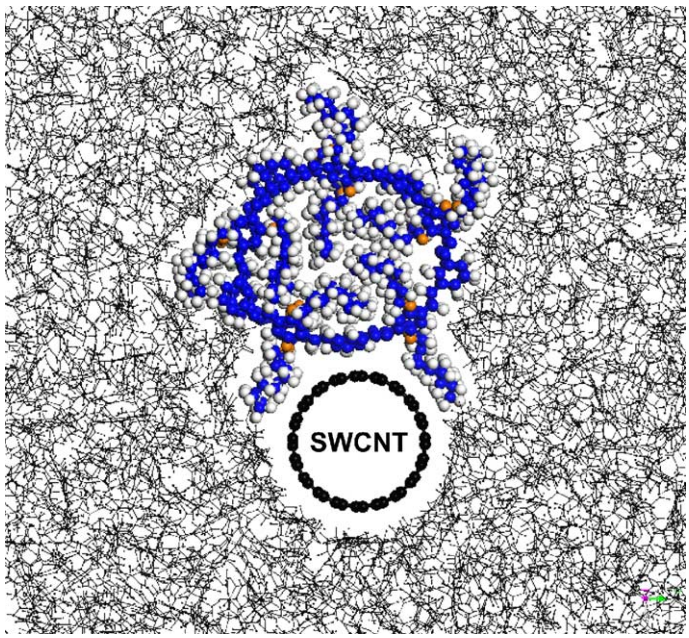

Fig. 7. Loose PmPV-DOctOPV conformation near a (10,10) SWCNT in toluene. A view along the SWCNT axis.

Table 2
Energy values obtained during computation of the binding energy between PmPV-DOctOPV and SWCNT in vacuum

Energy (kJ/mol) SWCNT	PmPV-DOctOPV conformation	Energy (kJ/mol)		Binding energy (kJ/mol) monomer PmPV-DOctOPV
		PmPV-DOctOPV	PmPV-DOctOPV + SWCNT	
68,515.2	Loose	−2,059.4	66,034.4	−28.1
68,515.2	Tight	−701.0	67,449.3	−45.6
68,515.2	Flat	−154.7	68,109.3	−125.6

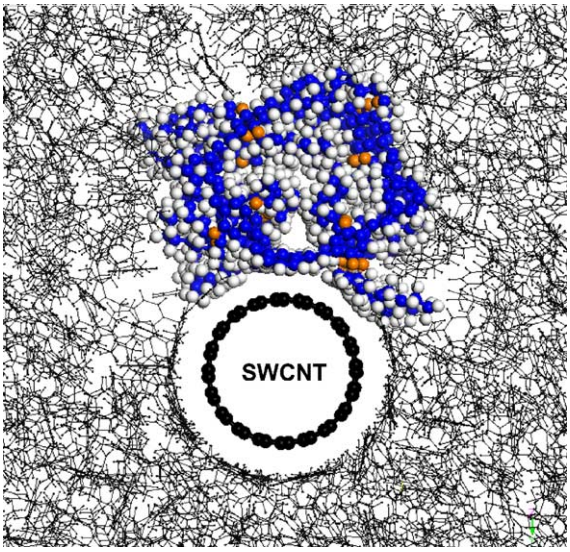

Fig. 8. Tight PmPV-DOctOPV conformation near a (10,10) SWCNT in toluene. A view along the SWCNT axis.

This finding is sometimes used to explain why the presence of PmPV-DOctOPV promotes solubilization of the SWCNTs in toluene. However, toluene may affect the binding energy between the PmPV-DOctOPV and the SWCNTs and hence, its role in the toluene in solubilization of the SWCNTs functionalized with PmPV-DOctOPV must be considered.

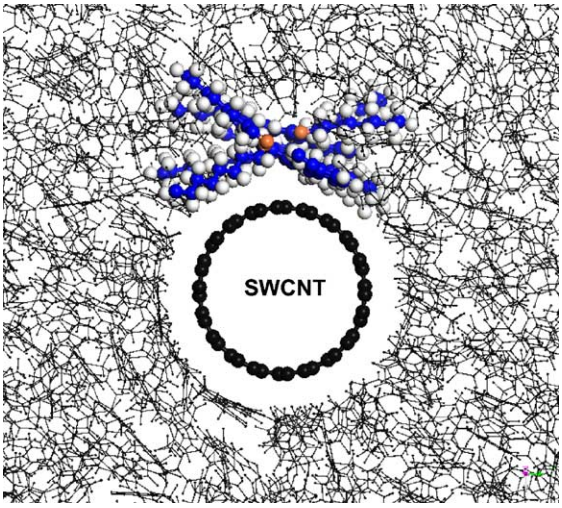

Fig. 9. Flat PmPV-DOctOPV conformation near a (10,10) SWCNT in toluene. A view along the SWCNT axis.

To properly model the process of solubilization of the SWCNTs functionalized with PmPV-DOctOPV in toluene and, in particular, the stability of the resulting homogeneous suspension (obtained via processes such as the sonication of the PmPV-DOctOPV and carbon nanotube bundles in toluene), an energy change accompanying the potential decomposition of the suspension is computed. Toward that end, the energy of unit cell containing a SWCNT, a PmPV-DOctOPV and toluene is first calculated. The values obtained for the three PmPV-DOctOPV conformations (given in the fourth column in Table 3) are then taken to represent the energy level of the SWCNT + PmPV-DOctOPV + toluene system in a well-sonicated state. Next, the SWCNTs are assumed to fall out of the suspension yielding a heterogeneous solution in which PmPV-DOctOPV is still well dispersed, but separated from the SWCNTs. Initially as this suspension decomposition process takes place, the SWCNTs which have fallen out of the solution fall to the bottom of the solution container but remain well separated. Therefore, the suspension in its decomposed state is considered to consist of well-separated PmPV-DOctOPV molecules and well separated (un-functionalized) SWCNTs. The energy of the suspension in this state is been calculated using the unit cell containing PmPV-DOctOPV + toluene and the one containing SWCNTs + toluene (the results are given in columns 1 and 3 in Table 3).

The difference in the energy of the suspension in its decomposed and its fully homogenized states, expressed per one monomer of the PmPV-DOctOPV, is given in the last column in Table 3 and is a measure of tendency of the suspension to decompose. Since these values are positive for all three conformations of the PmPV-DOctOPV, the suspension of SWCNTs functionalized with PmPV-DOctOPV in toluene has a lower energy and can be considered, on an energy basis, as stable. Also, the results given in Tables 2 and 3 suggest that the flat conformation of the PmPV-DOctOPV gives rise to the largest stability of a well homogenized SWCNT + PmPV-DOctOPV + toluene suspension with respect to a phase separation (decomposition).

As discussed above, as the SWCNT + PmPV-DOctOPV + toluene suspension undergoes a decomposition, the SWCNTs fall to the bottom of the container. Consequently there is some possibility for

Table 3
Energy values obtained during computation of the energy change accompanying the separation of single SWCNTs from a homogenized SWCNT + PmPV-DOctOPV + toluene suspension

Energy (kJ/mol) SWCNT + toluene	PmPV-DOctOPV conformation	Energy (kJ/mol)		Energy change (kJ/mol) monomer PmPV-DOctOPV
		PmPV-DOctOPV + toluene	PmPV-DOctOPV + SWCNT + toluene	
49,259.7	Loose	−22,936.1	26,005.8	21.18
49,259.7	Tight	−20,946.0	28,084.5	28.65
49,259.7	Flat	−20,482.0	28,692.6	42.55

re-assemble of the SWCNTs into bundles at the bottom of the container. Due to limitations of the computational resources available for the present work, only a cluster consisting of three SWCNTs suspended in toluene is analyzed. However, this is not considered as a major limitation since the concentration of the SWCNTs in toluene is generally very small (typically less than 1 wt.%) and, hence, one does not expect formation of very large SWCNT clusters at the bottom of the container. Optimized atomistic structures of a three-SWCNT cluster in toluene is shown in Fig. 10. The energy change associated with decomposition of a homogenized suspension of SWCNTs functionalized with PmPV-DOctOPV in toluene into a suspension of the PmPV-DOctOPV in toluene and a suspension of the three-SWCNT clusters suspended in toluene is computed using a procedure analogous to the one described above. The values obtained are given in Table 4. The results given in Table 4 shows that the energy changes associated with

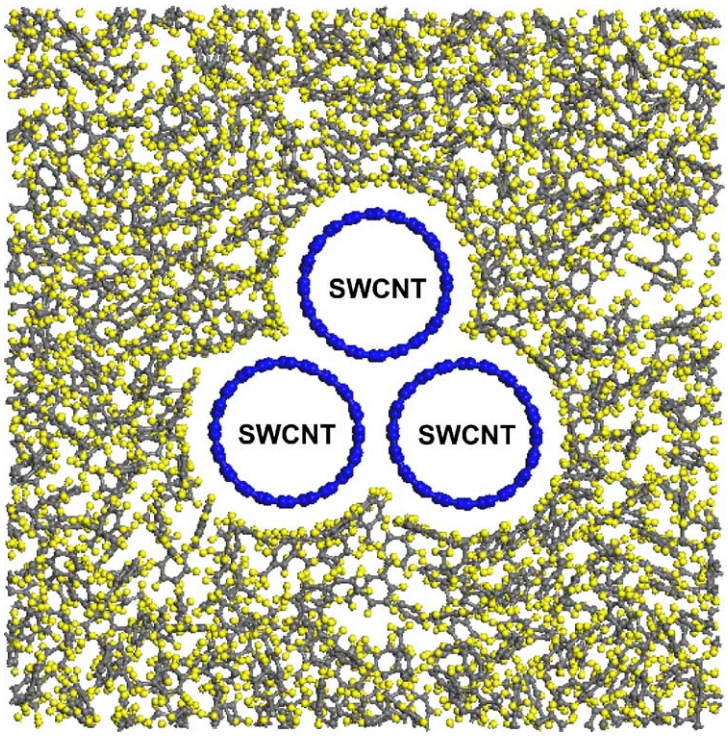

Fig. 10. Optimized atomistic configuration of a three-SWCNT cluster in toluene.

Table 4
Energy values obtained during computation of the energy change accompanying the separation of three-SWCNT clusters from a homogenized SWCNT + PmPV-DOctOPV + toluene suspension

Energy (kJ/mol) Three-SWCNT + toluene	PmPV-DOctOPV conformation	Energy (kJ/mol)		Energy change (kJ/mol) monomer PmPV-DoctOPV
		PmPV-DOctOPV + toluene	PmPV-DoctOPV + SWCNT + toluene	
147,686.1	Loose	−68,808.3	78,017.4	19.12
147,686.1	Tight	−62,838.0	84,253.5	24.77
147,686.1	Flat	−61,446.0	86,077.8	27.05

decomposition of the suspension are positive for all-three conformations of the PmPV-DOctOPV. Thus, a suspension of the SWCNTs functionalized with PmPV-DOctOPV in toluene can be considered as stable even with respect to formation of SWCNT clusters. Less positive values of the decomposition energies in the case of three-SWCNT clusters (Table 4), relative to the corresponding values for the single SWCNTs, (Table 3) can be attributed to the inter-nanotube binding energy.

A comparison of the corresponding results shown in Tables 3 and 4 suggests that the suspension becomes less stable as the number of SWCNTs in the clusters increases. While one may speculate that the suspension may become unstable with respect to a decomposition into large SWCNT clusters, it should be noted that the initial stage of decomposition of a SWCNT + PmPV-DOctOPV + toluene suspension is dominated formation of the well-separated single SWCNTs for which the decomposition energy is positive. Thus, this suspension can be generally considered as stable, which is in full agreement with the experimental observations (e.g. [9]).

4. Conclusions

Based on the results obtained in the present work, the following main conclusions can be drawn:

1. A toluene suspension of the SWCNTs (sidewall) functionalized with PmPV-DOctOPV is stable with respect to separation of the SWCNTs and hence can be used for decomposition of the nanotube clusters into individual SWCNTs.
2. Between the loose, tight, and flat conformations of PmPV-DOctOPV, the flat one is the most stable when used for sidewall functionalization of the SWCNTs in both vacuum and toluene.
3. The flat conformation of the PmPV-DOctOPV is the least stable conformation in both vacuum and toluene when the PmPV-DOctOPV is present as isolated molecules.

Acknowledgements

The material presented in this paper is based on work supported by the U.S. Army Grant number DAAD19-01-1-0661. The authors are indebted to Drs. Fred Stanton, Bonnie Gersten and William DeRosset of ARL for the support and a continuing interest in the present work.

References

[1] S. Iijima, Nature 354 (1991) 56.
[2] M. Grujicic, G. Cao, B. Gersten, Appl. Surf. Sci. 206 (2003) 167.
[3] S.J. Tans, R.M. Verschueren, C. Dekker, Nature 393 (1999) 40.
[4] A.C. Dillon, K.M. Jones, T.A. Bekkedahl, C.H. Kiang, D.S. Bethune, M.J. Heben, Nature 386 (1997) 377.
[5] M.M.J. Treacy, T.W. Ebbesen, J.M. Gibson, Nature 381 (1996) 678.
[6] P.G. Collins, K. Bradley, M. Ishigsmi, A. Zettl, Science 287 (2000) 1801.
[7] J.N. Coleman, A.B. Dalton, S. Curran, A. Rubio, A.P. Davey, A. Drury, B. McCarthy, B. Lahr, P.M. Ajayan, S. Roth, R.C. Barklie, W.J. Blau, Adv. Mater. 12 (2000) 213.
[8] M. in het Panhuis, A. Maiti, A.B. Dalton, A.V.D. Noort, J.N. Coleman, B. McCarthy, W.J. Blau, J. Phys. Chem. B 107 (2003) 478.
[9] B. McCarthy, J.N. Coleman, R. Czerw, A.B. Dalton, M. in het Panhuis, A. Maiti, A. Drury, H.J. Byrne, D.L. Carroll, W.J. Blau, J. Phys. Chem. B 106 (2002) 2210.

[10] A. Drury, S. Maier, A.P. Davey, A.B. Dalton, J.N. Coleman, H.J. Byrne, W.J. Blau, J. Synth. Met 119 (2001) 151.
[11] S. Curran, P. Ajayan, W. Blau, D. Carroll, J. Coleman, A. Dalton, A.P. Davey, B. McCarthy, A. Strevens, Adv. Mater. 10 (1998) 1091.
[12] S. Curran, A.P. Davey, J. Coleman, A. Dalton, B. McCarthy, S. Maier, D. Gray, M. Brennan, K. Ryder, M.L. de la Chapelle, C. Journet, P. Bernier, H.J. Byrne, D. Carroll, P.M. Ajayan, S. Lefrant, W.J. Blau, Synth. Met. 103 (1999) 2559.
[13] J. Coleman, A. Dalton, S. Curran, A. Rubio, A. Davey, A. Drury, B. McCarthy, B. Lahr, P. Ajayan, S. Roth, R. Barklie, W. Blau, Adv. Mater. 12 (2000) 213.
[14] A.B. Dalton, C. Stephan, J.N. Coleman, B. McCarthy, P.M. Ajayan, S. Lefrant, P. Bernier, W.J. Blau, H.J. Byrne, J. Phys. Chem. B. 104 (43) (2000) 10012.
[15] A.B. Dalton, W.J. Blau, G. Chambers, J.N. Coleman, K. Henderson, S. Lefrant, B. McCarthy, C. Stephan, H.J. Byrne, Synth. Met. 121 (1-3) (2001) 1217.
[16] B. McCarthy, J.N. Coleman, S.A. Curran, A.B. Dalton, A.P. Davey, Z. Konya, A. Fonseca, J.B. Nagy, W.J. Blau, J. Mater. Sci. Lett. 19 (2000) 2239.
[17] M. Grujicic, G. Cao, W. Roy, Atomistic simulations of solubilization of single-walled carbon nanotubes in toluene, J. Mater. Sci. 39 (2004).
[18] V. Lordi, N. Yao, J. Mater. Res. 15 (2000) 2770.
[19] W. Blau, Chem. Eng. News 6 (1999) 37.
[20] H. Sun, J. Phys. Chem. B. 102 (1998) 7338.
[21] H. Sun, P. Ren, J.R. Fried, Computat. Theor. Polym. Sci. 8 (1/2) (1998) 229.
[22] D. Rigby, H. Sun, B.E. Eichinger, Polym. Inter. 44 (1998) 311–330.